Structure
Article

Multimeric Options for the Auto-Activation of the *Saccharomyces cerevisiae* FAS Type I Megasynthase

Patrik Johansson,[1,*] Barbara Mulinacci,[1] Caecilia Koestler,[1] Ronnald Vollrath,[1] Dieter Oesterhelt,[1] and Martin Grininger[1,*]
[1]Department of Membrane Biochemistry, Max-Planck-Institute of Biochemistry, 82152 Martinsried, Germany
*Correspondence: johansso@biochem.mpg.de (P.J.), grininge@biochem.mpg.de (M.G.)
DOI 10.1016/j.str.2009.06.014

SUMMARY

The fungal type I fatty acid synthase (FAS) is a 2.6 MDa multienzyme complex, catalyzing all necessary steps for the synthesis of long acyl chains. To be catalytically competent, the FAS must be activated by a posttranslational modification of the central acyl carrier domain (ACP) by an intrinsic phosphopantetheine transferase (PPT). However, recent X-ray structures of the fungal FAS revealed a barrel-shaped architecture, with PPT located at the outside of the barrel wall, spatially separated from the ACP caged in the inner volume. This separation indicated that the activation has to proceed before the assembly to the mature complex, in a conformation where the ACP and PPT domains can meet. To gain insight into the auto-activation reaction and also into the fungal FAS assembly pathway, we structurally and functionally characterized the *Saccharomyces cerevisiae* FAS type I PPT as part of the multienzyme protein and as an isolated domain.

INTRODUCTION

Synthesis of long aliphatic acids is essential to living cells, not only for the construction of lipid membranes and the long-term storage of chemical energy, but also to supply precursors for many biologically important molecules. Nature employs two main schemes for de novo production of fatty acids. Eukaryotes generally use the fatty acid synthase system I (FAS I), which is composed of large multifunctional enzymes that catalyze all the necessary reactions for fatty acid synthesis. In contrast, most prokaryotes instead use the distributed FAS II system, consisting of a set of separate enzymes, each catalyzing one of the steps of the FAS cycle. In both systems, the acetyl and malonyl substrates are transferred onto a 4′-phosphopantetheine group of an acyl carrier protein (ACP) that guides the intermediates of fatty acid synthesis through the reaction cycle (Schweizer and Hofmann, 2004).

According to the type of synthesis, ACPs of the dissociated FAS type II systems are separate proteins, whereas FAS type I ACPs are covalently linked to the multienzyme complexes. Fusion of the ACP to the rest of the fatty acid synthase domains leads to increased local concentrations of the ACP bound intermediates, dramatically increasing the rates of synthesis (Lynen, 1980; Spivey and Ovadi, 1999). However, before the ACP can start to deliver its substrates, it has to be posttranslationally modified by the addition of a prosthetic carrier-group. This activation of the FAS is performed by a specific phosphopantetheine transferase enzyme (PPT) that covalently attaches the phosphopantetheine moiety of coenzyme A (CoA) onto a conserved serine residue of the ACP (Elovson and Vagelos, 1968; Lambalot and Walsh, 1995) (Figure 1A).

Recently, detailed insight has been gained into the type I fatty acid synthases by a number of X-ray crystal structures. These have shown that the FAS multienzyme proteins of higher and lower eukaryotes exhibit considerably different architectures. The mammalian FAS is composed of a single multidomain chain, forming a 540 kDa X-shaped dimeric structure (Maier et al., 2008). In contrast, the fungal FAS is organized in either one or two (α/β) multidomain proteins, which assemble to highly symmetric, 2.6 MDa large, hexameric or heterododecameric ($\alpha_6\beta_6$) complexes, respectively (Jenni et al., 2007; Johansson et al., 2008; Leibundgut et al., 2007; Lomakin et al., 2007). One of the major functional differences of these FAS complexes is the mechanism of the posttranslational modification of the ACP domain. While the activation of the mammalian FAS is performed by a separate PPT enzyme, many of the fungal FAS multienzymes harbor a PPT domain fused to the C terminus of the α chain, and are able to perform an auto-activation of ACP (Figure 1B) (Fichtlscherer et al., 2000).

Compared with the catalytic domains part of the fatty acid cycle and the ACP inside the fungal $\alpha_6\beta_6$ FAS particle, the fused PPT domain was found to be located at the outside of the barrel-like structure, separated from its ACP partner by ~60 Å and by the rigid barrel wall (Lomakin et al., 2007) (see Figure 1B). This spatial separation seems to have dramatic consequences for the formation process of the fungal FAS megasynthase. If the posttranslational modification of the ACP cannot take place in the mature FAS particle, a structural organization prior to the $\alpha_6\beta_6$ assembly has to exist in which the activation step can proceed. Any conformation competent for activating the *S. cerevisiae* FAS has to fulfill two basic criteria: (1) the PPT and ACP domains have to be able to meet, and (2) PPT has to be active.

The PPT-related enzymes of eukaryotes and bacteria have been grouped into two classes (Copp and Neilan, 2006; Lambalot et al., 1996). The first class is exemplified by the *Bacillus subtilis* surfactin synthase (Sfp), an enzyme of about 25 kDa with a 2-fold pseudosymmetry (Reuter et al., 1999). This class also includes the peptidyl carrier proteins of nonribosomal peptide

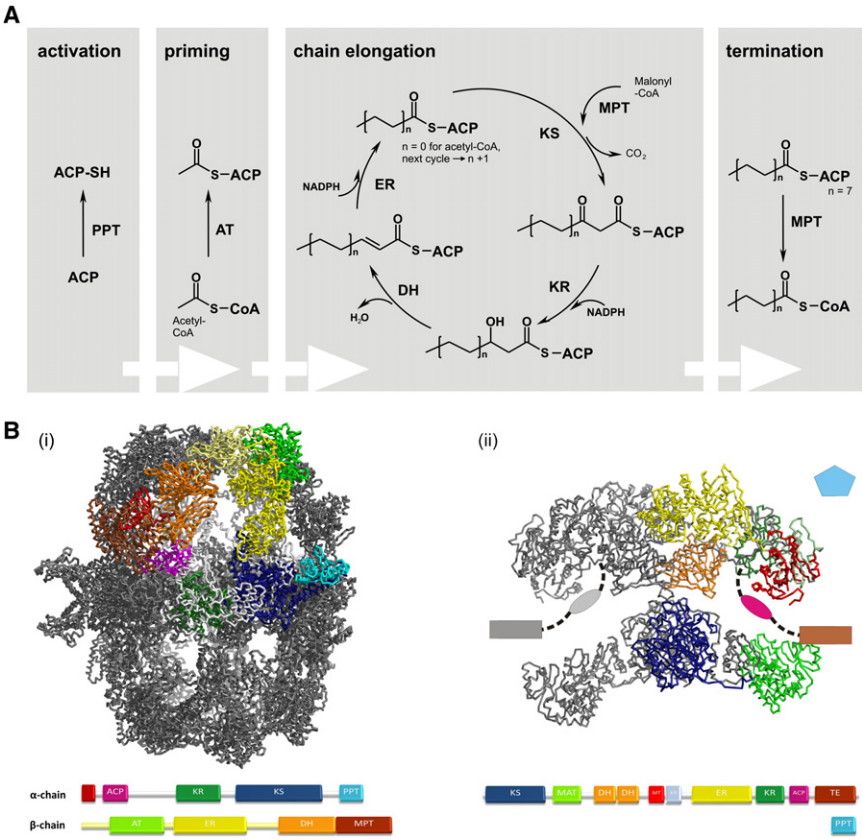

Figure 1. Fatty Acid Synthesis

(A) Catalytic competence of the fungal type I fatty acid synthase. The activation, priming, elongation, and termination of fungal FAS is carried out by seven domains: a phosphopantetheine transferase (PPT), an acetyl transferase (AT), a malonyl/palmitoyl transferase (MPT), a ketoacyl synthase (KS), a ketoacyl reductase (KR), a dehydratase (DH), and an enoyl reductase (ER). To highlight the active thiol function of the pantetheine tail, CoA and phosphopantetheinylated ACP are denoted CoA-SH and ACP-SH, respectively.

(B) Structure and domain organization of the fungal (i) and mammalian (ii) FAS type I systems. Single chains of fungal and mammalian FAS type I complexes have been colored according to the attached domain overview. In addition to the overlapping domains of the fungal FAS, the mammalian system also harbors a malonyl/acetyl transferase (MAT) and a thioesterase (TE) domain, as well as a methyltransferase (*MT*) and a *KR* pseudodomain. The mammalian PPT and the flexible TE and ACP domains were not solved together with the complex. High-resolution structures of the isolated domains are available with PDB entry codes 2CG5, 1XKT, and 2PNG, respectively (Bunkoczi et al., 2007; Ploskon et al., 2008; Chakravarty et al., 2004).

synthases (NRPSs), as well as enzymes like the human PPT (Joshi et al., 2003) and the Lys5 phosphopantetheine transferase (Ehmann et al., 1999). Sfp-like PPTs are active as monomers with the active site formed between the two PPT folds of the pseudodimer. The second class of PPTs, the holo-acyl carrier protein synthases (AcpS), are responsible for the phosphopantetheinylation of the bacterial FAS type II ACPs. They are significantly smaller (13 kDa) than the Sfp-like PPTs and are active as trimers (Lambalot and Walsh, 1995). In spite of the differences in size and the overall low sequence similarity within the PPT superfamily, the AcpS-like PPTs share striking structural similarities with the Sfp-like PPTs, with a conserved CoA-binding site at the interface of the monomers.

Only limited data about the function of PPTs that appear as integrated domains of the fungal FAS are currently available. This is partly a result of the size of the multienzyme assemblies, making the phosphopantetheinylation reaction difficult to monitor (Fichtlscherer et al., 2000; Crawford et al., 2008a). In addition, the PPT domains of the published *S. cerevisiae* and *Thermomyces lanuginosus* low-resolution FAS models were either absent or not reliably built because of their flexible attachment at the outside of the barrel-shaped complex (Lomakin et al., 2007).

To analyze the working mode of the fused FAS type I PPTs and to get insight into the auto-activation reaction of the *S. cerevisiae* FAS, we have determined the high-resolution crystal structure of the individual PPT domain with and without its CoA ligand, and we have performed biochemical studies on the phosphopantetheinylation reaction. Our structural and functional data indicate that the FAS type I PPT domain requires a dimeric or a trimeric state for catalytic activity. This finding, together with the PPT/ACP interaction requirement, puts some fundamental constraints on the auto-activation reaction and potentially also on the assembly of the $\alpha_6\beta_6$ *S. cerevisiae* FAS megasynthase.

RESULTS

The Fungal FAS Type I PPT

To characterize the PPT domain and its potential states of oligomerization, a C-terminal 13 kDa segment of the FAS α chain (G1768–K1887) was cloned, expressed, and purified using a cleavable His(6)-tagged construct. In contrast to the monomeric state of PPT seen in the native FAS multienzyme (Johansson et al., 2008; Lomakin et al., 2007), size exclusion chromatography on the separated domain indicated a trimeric oligomerization with some tendency to form hexamers (see Figure S1 available with this article online).

The X-ray structure of the CoA-free PPT domain was solved to a resolution of 1.9 Å, and the structure of the PPT/CoA complex was solved to a resolution of 2.2 Å. The PPT fragment folds into an elongated structure formed by a long α-helix (α55), which is sandwiched between an extended antiparallel three-stranded β sheet at the local three-fold axis (β41/β44/β45) and a short antiparallel two-stranded β sheet (β42/β43) accompanied by three helices at the outer surface (α53/α54/α56). Compared with the known AcpS enzymes from bacteria and protozoa, the FAS type I PPT is lacking helix α1, between β1 and α2 (β41 and α53

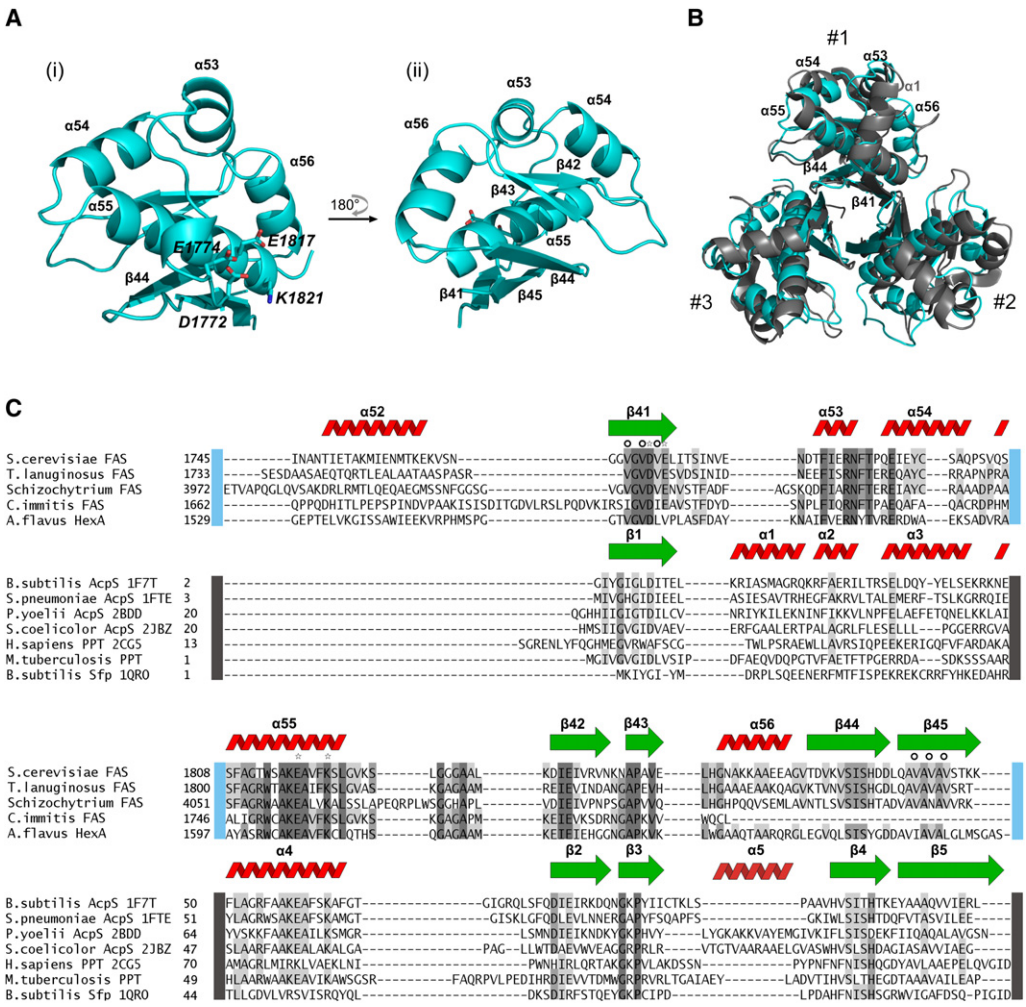

Figure 2. FAS Type I PPT

(A) Monomer of the FAS type I PPT with the active site residues D1772, E1774, E1817, and K1821 shown.

(B) Superposition of the trimers of the fungal FAS type I PPT and the *B. subtilis* AcpS (gray, PDB-code 1F7T). View along the hydrophobic valine channel. Protomer 1 (#1) is oriented as the PPT monomer in Figure 2A(i).

(C) Grouped structure-based sequence alignment of five fungal FAS type I/HexA PPT domains (cyan colored bar) and a number of pro- (Chopra et al., 2002) and eukaryotic (Vedadi et al., 2007) type I and II homologs (gray bar). The active site residues shown in Figure 2A are highlighted with stars and the valine-repeat forming the hydrophobic channel with circles.

of FAS type I PPT), similar to the pseudodimeric Sfp protein from *B. subtilis* (PDB-code 1QR0; Reuter et al., 1999). Helix α5 between β3 and β4, which is not consistently found in AcpS-like PPTs, is present in the PPT domain as helix α56 between β43 and β44 (Figures 2A and 2B; Figure S2A).

In line with the AcpS proteins, the PPT trimer is constructed by a nine-stranded antiparallel β-barrel structure, formed by β41 of one monomer packing onto β44 and β45 of another, burying a total surface area of about 1750 Å^2. The inner surface of the generated 35 Å channel is highly hydrophobic, including a core of 18 repeated valine side chains. This is even more hydrophobic than many of the bacterial homologs, indicating an importance of this motif in the FAS type I PPTs (Figure 2C).

In both crystal forms, the PPT domains pack as a dimer of trimers, potentially reflecting the hexameric state found in the size-exclusion results. However, the crystallographic trimer-trimer contacts are solely formed by hydrogen bonds between nonconserved side chains, indicating that the hexamer is of little physiological relevance (Figure S2B).

CoA Binding in the Fungal FAS Type I PPT

Similar to the bacterial counterparts, the PPT catalytic site is located at the dimeric interfaces of the PPT trimer (Figure 3A) (Chirgadze et al., 2000; Parris et al., 2000). As seen in the 2.2 Å PPT/CoA complex structure, the coenzyme ligand is bound in an overall bent conformation with the pyrophosphate group at its apex. The 3′,5′ADP substructure of CoA fits into a pocket made up by loop α55–β42, as well as β44 and loop β42–β43 of the neighboring monomer (Figure 3B). Similar to the AcpS and Sfp/human PPT proteins (Bunkoczi et al., 2007; Parris et al., 2000; Reuter et al., 1999), the ribose adopts an $C_{3'}$-*endo* conformation with the equatorially positioned 3′phosphate placed in

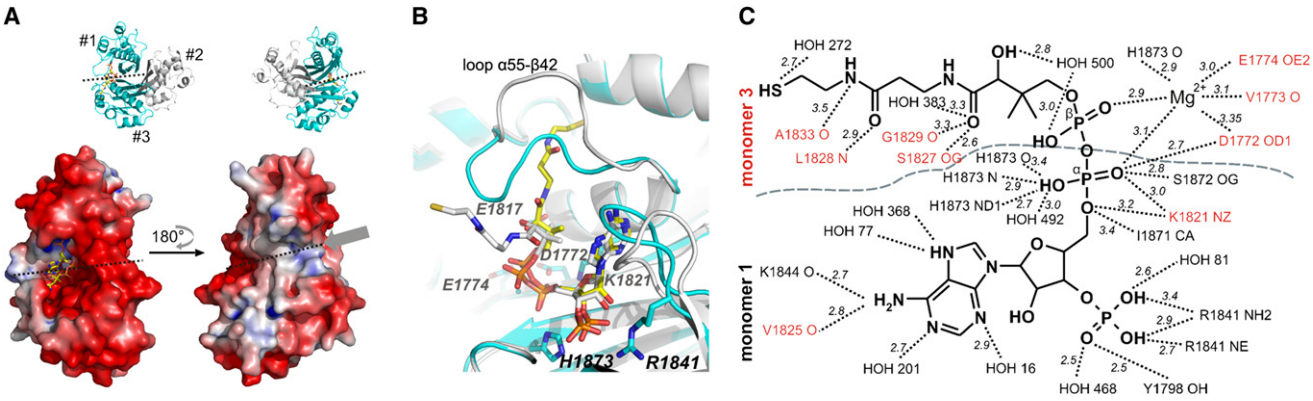

Figure 3. FAS Type I PPT Active Site

(A) Surface potential representation of a PPT dimeric subunit, calculated with the ABPS plug-in of PYMOL (www.pymol.org). Red color indicates negative charges, and blue color indicates positive charges, ranging from −3 to +3 kcal/e.u. charge units. The CoA-binding site in the shallow groove formed by two monomers is colored in yellow. The dashed line delineates interacting monomers, whereas the arrow indicates the valine rich hydrophobic channel. A cartoon representation of the PPT, highlighting the surface represented dimer in cyan is attached.

(B) CoA-binding site of the fungal FAS type I PPT. Superposition of two symmetry related molecules shows the different conformations of the phosphopantetheine tail and loop α55–β42 found in the PPT/CoA complex. The CoA molecule depicted in white forms a disulfide bridge to CoA of a neighboring PPT hexamer in the crystal lattice.

(C) Details of the interaction between the fungal FAS type I PPT and CoA. Labels in black and red as well as the dashed line indicate contributions from two protomers of the trimeric arrangement (see also Figure 3A).

the cationic depression of the CoA-binding pocket. In contrast, the CoA phosphopantetheine adopts a significantly different conformation than in the reported PPT/CoA complex structures. In the FAS type I PPT, the extended loop between α55 and β42 wraps around the phosphopantetheine tail, forcing atoms PO9/PO10 into an eclipsed conformation (Figure S3A).

The CoA predominantly binds to the PPT dimer interface via its nucleotide part, with 12 of 16 polar interactions being related to the 3′,5′ADP submoiety. As illustrated in Figure 3C, the interactions to the nucleotide part are almost exclusively contributed by one of the two monomers forming the cofactor-binding site, while the pantetheine tail is interacting with the other monomer. The β-phosphate of the CoA pyrophosphate moiety is not in direct contact with the protein. This loose binding of the phosphopantetheine moiety is consistent with the chemistry of the reaction in which the phosphopantetheine of CoA is transferred on the ACP, while the 3′,5′ADP group remains bound to the PPT. The lack of restraints on the phosphopantetheine is reflected by a different conformation of CoA found in one of the six PPT molecules of the crystallographic asymmetric unit. This CoA forms a disulfide bond with another phosphopantetheine tail, trapping it in a favorable PO9/PO10 staggered conformation (see Figure S3A).

Mg^{2+} Coordination and the Phosphopantetheinylation Reaction

The phosphopantetheinylation reaction proceeds in three steps: (1) deprotonation of the ACP active site serine (Ser + B^- → Ser^- + BH), (2) SN_2 type nucleophilic attack on the β-phosphate of the bound CoA molecule (Ser^- + CoA → Ser-phosphopantetheine + 3′,5′ADP^-), and (3) protonation of the α-phosphate of 3′,5′ADP by a lysine conserved in the PPT proteins (3′,5′ADP^- + $LysH^+$ → 3′,5′ADP + Lys). The transferase reaction has been shown to require a Mg^{2+} ion, coordinated at the active site in both the bacterial AcpS and the human PPT enzymes (Elovson and Vagelos, 1968; Lambalot and Walsh, 1995, Bunkoczi et al., 2007). As both phosphates of CoA are involved in the coordination, no density of a divalent ion could be seen in averaged 2Fo-Fc or Fo-Fc maps of the CoA-free PPT, in spite of a 10-fold molar excess of magnesium used for crystallization. In contrast, X-ray data of the PPT/CoA complex showed electron density at the Mg^{2+} site. However, structure bond lengths of Mg^{2+} and its chelating ligands were found to exceed expected values. As no other cations except Na^+ were present during crystallization, the observed coordination pattern is a likely consequence of the acidic conditions (pH 4) used for PPT/CoA crystallization, protonating the chelating carboxy groups (Figure S3B).

The coordination pattern of the magnesium ion is critical for the mechanism of the phosphopantetheine transferase reaction, as ligands of the Mg^{2+} account for the initial deprotonation step generating the ACP serine nucleophile (reaction 1). In the AcpS proteins, the proton abstraction is achieved by one of the three waters coordinated to the Mg^{2+} (Parris et al., 2000). In contrast, for human PPT, the side chain of E181, located at Mg^{2+} coordination distance, has been suggested to act as a base, abstracting a proton from the ACP serine (Bunkoczi et al., 2007). Because of the acidic conditions of PPT/CoA crystallization, the discussion of the reaction mechanism on the basis of the X-ray data is difficult. However, as E1817, the equivalent to the active glutamate of human PPT (E181), is not involved in Mg^{2+} coordination, and the densely coordinated Mg^{2+} might not allow the coordination of an *active* water molecule, it is tempting to speculate that E1774, conserved in fungal type I PPTs, deprotonates ACP S180. Interestingly, such an alternative mechanism could also apply for Sfp from *B. subtilis*, where the Mg^{2+} binding pattern is almost identical to the *S. cerevisiae* PPT, with the side chains E1817/D1772/E1774 corresponding to E151/D107/E109 of the Sfp (Reuter et al., 1999).

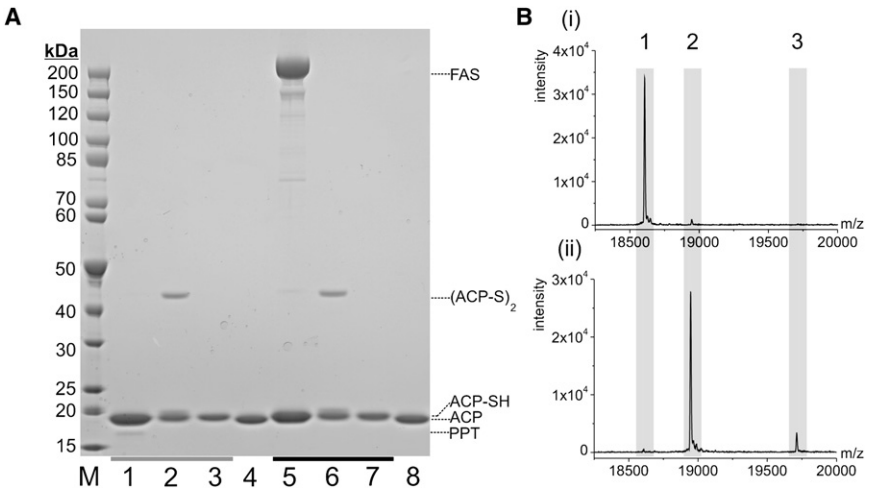

Figure 4. PPT Activity Assay

(A) 4%–12% Bis/Tris SDS-PAGE gel (NuPage, Invitrogen) showing the turnover of apo-ACP into holo-ACP (ACP-SH). Holo-ACP tends to dimerize via a disulfide linkage, giving $(ACP\text{-}S)_2$. However, the disulfide bond is cleaved under the reducing conditions of the sample loading buffer. The gray bar highlights the samples of reaction with the separate PPT domain, and the black bar highlights the samples of the reaction with the mature *S. cerevisiae* FAS complex. Lane M, marker; lanes 1 and 5, reaction solution; lanes 2 and 6, ACP purified from the reaction solution and loaded on gel under nonreducing conditions; lanes 3 and 7, same as lanes 2 and 6 but loaded on gel under reducing conditions; and lanes 4 and 8, ACP apoprotein reference.

(B) Mass spectrometric analysis of ACP. In *E. coli*, ACP is expressed in its apo-state (i). After 3 hr, apo-ACP is quantitatively turned over to holo-ACP (ii) by PPT as separate protein or attached to the FAS particle. His-tagged proteins ACP_H(6) and PPT_H(6) were used for the activity assay. Apo-ACP_H(6) 18 606 Da; holo-ACP_H(6) 18 947 (18 606(−1) + 342 (phosphopantetheine)); holo-ACP_H(6) covalently binding CoA via disulfide bridging 19 712 (18 606(−1) + 342(−1) + 767(−1) (CoA)).

Phosphopantetheinylation Activity of the Separate FAS Type I PPT Domain

Although the capability for auto-activation of the fungal FAS had already been suggested by complementation studies (Fichtlscherer et al., 2000), previous attempts to directly monitor the phosphopantetheinylation reaction using discrete domains failed, potentially as a result of misplaced domain borders (Lambalot et al., 1996). To test the enzymatic activity of the FAS type I PPT, we used His(6)-tagged ACP and PPT constructs (ACP_H(6) and PPT_H(6)). Similar to the construct used for crystallization, heterologously expressed His-tagged PPT eluted as trimers with a small hexameric fraction. The ACP domain eluted as a monomer from size-exclusion chromatography and was found by mass spectroscopy to express and purify in its apo-form (see Figure S1). This inability of the *E. coli* host to activate the heterologously expressed FAS type I ACP correlates well with the different binding strategies of bacterial and fungal PPTs (see below).

As shown in Figures 4A and 4B, the separate PPT domain was readily able to convert ACP (apo) into ACP-SH (holo). To support the multimeric requirement of PPT as implied from the X-ray structural data, mutational studies on the isolated PPT domain were performed. With the aim of generating monomeric PPT, we mutated the hydrophobic valine channel. As listed in Table 1, the mutations at the valine channel, V1769D/V1771S/V1773L and V1769D/V1771S/V1773L/V1879S/V1881E, did not induce a dissociation of the trimeric state. However, in spite of keeping the oligomeric integrity, the valine channel mutants were catalytically inactive, suggesting that the disturbed oligomerization allosterically affected the PPT activity (see for example Boulanger and Kantrowitz, 2003). The sensitivity toward the valine channel and modifications at the N terminus of the PPT domain are consistent with a strong decrease of phosphopantetheinylation activity reported for the I2A and I5R mutation of the *B. subtilis* AcpS (N1766 and V1769 of *S. cerevisiae* FAS) (Parris et al., 2000) and the inactivity of a *S. cerevisiae* G1770D FAS α chain mutant (Fichtlscherer et al., 2000). Similar to the other mutants at the hydrophobic channel, a G1770D mutation in the separate PPT did not affect the trimeric behavior but completely abolished transferase activity. However, as residues around position 1770 are close to the active site, the loss of catalytic ability can also be due to reduced CoA binding.

To get experimental insight into the multimeric requirement for the FAS type I PPT activity while avoiding allosteric effects, we performed a PPT complementation study. The structure of a PPT monomer shows that the 3′,5′ADP submoiety binding site is separated by 20 Å from the Mg^{2+}-binding site. Upon multimerization, two monomers in turn reconstitute the active site at the dimeric interface (see Figure 3C). PPT constructs mutated at the CoA-binding site (R1841A affecting 3′,5′ADP coordination) or mutated at the Mg^{2+}-binding site (D1772S/E1774S) were found not to be active. However, when mutants where mixed and dissociated/reassociated, catalytic activity could be regained. This result implies that neither of the two active site halves can independently catalyze the phoshopanteteheinylation reaction (such as in a putative monomeric state) and that multimerization is indeed a requirement for activity.

Phosphopantetheinylation Activity of the *S. cerevisiae* FAS Complex

Somewhat surprisingly, the mature $\alpha_6\beta_6$ FAS purified from *S. cerevisiae* was also found to be able to catalyze phosphopantetheinyl transfer to free ACP (see Figures 4A and 4B and Table 1). This was not expected from the crystal structure, as the location of the single PPT domain on the surface of the $\alpha_6\beta_6$ FAS particle indicated the PPT to be in a catalytically inactive state (Lomakin et al., 2007). The observed PPT activity could potentially be due to the temporary formation of a PPT dimer on the perimeter of the FAS barrel, supported by the flexibility of the PPT domains observed in X-ray and EM maps. Latent dimers could thereby be stabilized by the bridging effect of CoA, present in the reaction solution in an about 50-fold molar excess (see Figure 3C).

Because of the packing of two PPT monomers seen in the trimeric crystal structure, a PPT dimer on the FAS surface can

Table 1. FAS Type I PPT Mutant Studies

PPT species	MW calc [Da]	MW meas [Da][a]	MW [kDa][b]	ACP-SH [%][c]
$\alpha_6\beta_6$ FAS				98
PPT wild type			46.5	98
PPT G1770D	14024.6	14024.3	45.6	0
PPT DSL[d]	13984.5	13984.5	43.8	0
PPT DSL_SE[e]	14002.4	14002.4	47.4	0
PPT D1772S/E1774S	13896.5	13895.9	40.0	0
PPT R1841A	13881.5	13880.9	48.2	6
PPT D1772S/E1774S// R1841A			46.7	97

[a] Determined by mass spectrometry.
[b] Determined from gel filtration runs on a Superdex S200 16/60 in the last step of the PPT purification protocol.
[c] Relative quantification by total ion count as a mean of two values; see also Experimental Procedures.
[d] V1769D/V1771S/V1773L mutated PPT.
[e] V1769D/V1771S/V1773L/V1879S/V1881E mutated PPT.

be created only if the noncrystallographic two-fold axis of the FAS α_6-wheel is violated. Since β41 interacting with ACP during the activation reaction is facing the FAS main body, a functional ACP docking site could potentially be formed by a combined rotation/translation of each PPT domain by about 120° and 25 Å, centering the α56 side of the dimer on the $\alpha_6\beta_6$ dyad.

Updated Structural Model of the Fungal FAS

To investigate the detailed interactions between the PPT domain and the FAS $\alpha_6\beta_6$ barrel, the 13 kDa structure was docked into the weak density at the C terminus of the *S. cerevisiae* multienzyme complex (Figure 5A) (Johansson et al., 2008). The PPT domains pack as monomers onto the three four-helix bundles formed by the FAS ketoacyl synthase domains, separated by a distance of about 40 Å. A number of interactions between helices α44, α45, and α52 of the KS and β41, β44, and β45 of the PPT domain seem to shield the hydrophobic surface of the major sheet of the PPT from the bulk solvent. Apart from a several hydrophobic interactions, the side chains of E1464 and K1460 of the KS α44 are likely to form electrostatic interactions with the active site residues D1772, E1817, E1774, and K1821 of the PPT domain (Figure 5B). Although the highly charged active site residues of the PPT domain are retained throughout fungi, the α44, α45, and α52 helices are less conserved or even significantly truncated in some species. This small number of interactions with the main FAS particle correlates well with the observed flexibility of the *T. lanuginosus* and the *S. cerevisiae* FAS type I PPT domains, indicated by the crystal structures, and the missing density for PPT in EM maps (Jenni et al., 2007; Johansson et al., 2008).

Interaction Between the Fungal FAS Type I ACP and PPT

In the X-ray models of the *S. cerevisiae* FAS, the flexible ACP domains were found to be stalled at the KS domains, allowing the tracing of the fungal FAS type I ACP structure (Leibundgut et al., 2007; Lomakin et al., 2007; Johansson et al., 2008). In spite of a low sequence identity of 8% to the FAS type II ACP from *B.*

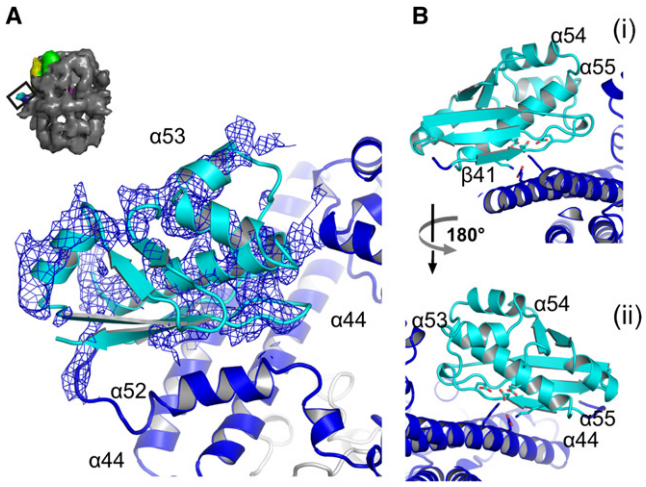

Figure 5. Updated Fungal FAS Model
(A) Docking of the high-resolution PPT monomer into the 4 Å maps *S. cerevisiae* FAS structure. Averaged omit 2Fo-Fc map is contoured at 1σ within 3 Å from the PPT. For orientation, a 20 Å electron microscopy model is shown as an inset (Johansson et al., 2008).
(B) Potential interactions of PPT E1774 as well as the PPT active residues D1772, E1817, and K1821 with K1460 and E1464 on helix α44.

subtilis, the FAS type I ACP features a similar helix bundle-like core structure as the bacterial ACPs (Parris et al., 2000; Roujeinikova et al., 2002). This fold is also seen in the vertebrate FAS type I system (Bunkoczi et al., 2007; Ploskon et al., 2008). However, in addition to the core fold, the fungal type I ACP has an extra C-terminal four-helix bundle domain, making it about twice the size of its bacterial and vertebrate counterparts. This added structural feature has been suggested to be important for the docking to the different functional domains of the FAS multienzyme, as exemplified by the ACP-KS interaction of the *S. cerevisiae* FAS structures (Leibundgut et al., 2007) (Figures 6A and 6B).

In the fungal FAS type I system, the PPT domain transfers the phosphopantetheine moiety of CoA onto the β-hydroxyl side chain of ACP S180, located on a loop between two helices of the core structure (α7 and α8, FAS numbering). In spite of the similar reaction, the details of the FAS type II, the vertebrate FAS type I, and the fungal FAS type I PPT/ACP binding seem to be quite different. In the bacterial ACPs, the side chain adjacent to the reactive S36, D35, forms a conserved salt bridge to R14 of the AcpS, shown to be essential for ACP recognition (*B. subtilis* ACP/AcpS numbering) (Keating et al., 2002; Zhang et al., 2003). In the fungal ACPs, this residue is altered to a lysine, K179, that instead is likely to make an electrostatic interaction with the conserved side chain of D1875 at the loop between PPT β44 and β45. The following α8 helix shows more conservation between the bacterial and fungal proteins. However, only the side chains interacting with the interior of the ACP are conserved, whereas almost all residues positioned to interact with the PPT domain are altered. The α8 helix of the FAS type I ACP is likely to coordinate with residues N184, K192, and K223 to residues N1790, W1813, F1786, E1782, and D1784 of the PPT, conserved throughout fungi. This interaction is different from both the mixed hydrophobic/electrostatic binding pattern of the bacterial FAS type II AcpS/ACP proteins (Parris et al.,

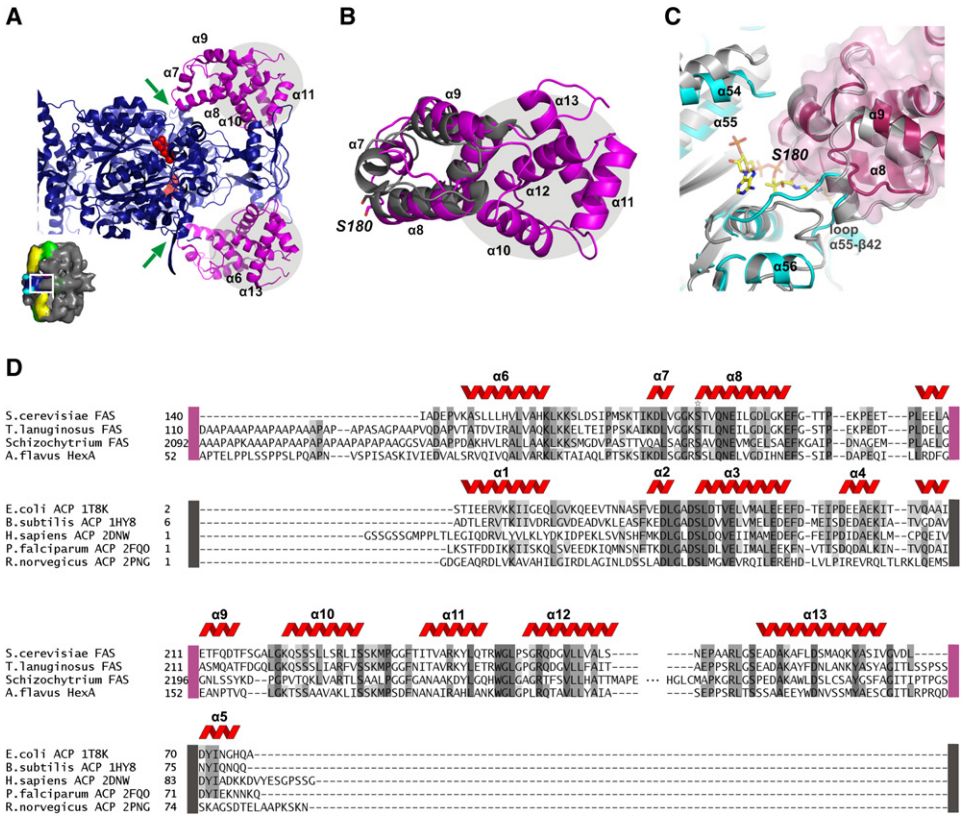

Figure 6. FAS Type I ACP

(A) Substructure of the FAS complex showing the ACP docked to the KS domain. For illustration of the KS active site, the FAS inhibitor cerulenin is shown in ball representation in red (Johansson et al., 2008). The phosphopantetheine entrance channels are indicated by green arrows, and the ACP docking domains are highlighted by a gray background. For orientation, a 20 Å electron microscopy model is shown as an inset (Johansson et al., 2008).

(B) Superposition of the FAS type I ACP on the *E. coli* ACP in its apo-form (PDB-code 1T8K). The active serine S36 of the bacterial ACP is shown.

(C) Superposition of the FAS type I PPT (cyan) and ACP (magenta) domains onto the *B. subtilis* AcpS/ACP complex (PDB-code 1F80) (white).

(D) Grouped structure-based sequence alignment of four fungal FAS type I/HexA ACP domains (magenta colored bar) and a number of pro- and eukaryotic FAS II ACPs (gray bar). S180 is highlighted (star).

2000) and the mainly hydrophobic binding observed in the mammalian FAS type I PPT/ACP system (Bunkoczi et al., 2007).

Because the backbone conformation of L159–K179 of the FAS type I ACP is altered, compared with the other known proteins, and because helix α4 of the bacterial ACPs is completely missing in the fungal domain, the detailed ACP/PPT interactions in this region are hard to predict. However, the changes in the FAS ACP seem to be adapted to the changes in the PPT. The conformation of the α7–α8 loop prior to the catalytic S180 of the FAS type I ACP might be adapted to the differing angle of PPT α54 and the different conformation of the following loop to α55. In the same way, the flexible G1824–L1834 loop between α55 and β42 of the PPT adopts a significantly more extended conformation than its bacterial counterparts, potentially wedging between α8 and the retracted α8–α9 loop (F194–P205) of the ACP (Figure 6C). As indicated by the PPT-substrate complex, such an interaction is likely to be mediated by the CoA, stabilizing the α55–β42 loop by its long phosphopantetheine tail.

Although the docking domain of ACP has been suggested to be involved in the specific interactions between ACP and the different FAS domains (Leibundgut et al., 2007), it does not seems to contribute to the PPT/ACP interface (Figure 7A), or to the oligomerization of the PPT domain during the activation reaction. However, the docking of the ACP domain is relevant for the orientation of the PPT/ACP interface relative to the main body of the *S. cerevisiae* FAS. Because the ACP binds to the α53/α54 face of PPT, this side has to be kept accessible for the bulky FAS type I ACP.

DISCUSSION

Multimeric Options for the Fungal FAS Type I PPT

Intriguingly, the FAS type I PPT domain seems to appear in several oligomeric states: (1) monomeric, as a domain held at the outside of the FAS structure; (2) dimeric, potentially accounting for the PPT activity of the mature FAS particle; and (3) trimeric, as a separate protein. The trimeric state is the intrinsic oligomeric form, whereas the monomeric and the proposed dimeric structures of PPT are clearly a consequence of the restricted flexibility of the PPT domains when anchored to the FAS complex.

As shown by the mutational studies, the FAS type I PPT needs to multimerize to be catalytically active. Consequently, the oligomeric state of the PPT during the auto-activation reaction is a

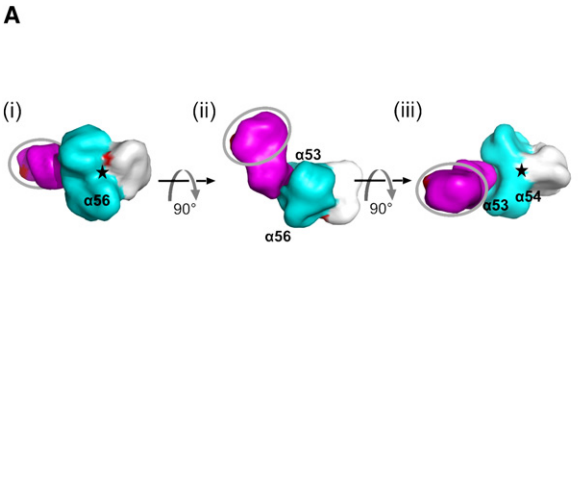

Figure 7. Restraints for the FAS Activation Reaction

(A) ACP/PPT docking with the fungal FAS type I PPT (cyan/white) in a dimeric (substructure in cyan) or trimeric oligomeric state. For clarity, ACP (magenta) is docked to just one of the three active sites. The three-fold axis of the PPT is indicated by a star. The C-terminal end of the ACP and N-terminal end of PPT domain are highlighted in red, representing the connection with the KR-KS sequence in a potential precomplex. The docking domain of ACP is encircled in gray (see also Figure 6A). A sphere with a probe radius of 10 Å was used for surface calculation.

(B) Putative α_6 interaction sites for ACP (magenta) and PPT (cyan), generating dimeric (1, 2) or trimeric (3) PPT. A potential posttranslational modification carried out by an α_6-wheel structure requires large movements of the ACP (1, 2) and/or the PPT (2, 3) domain. Moving distances for PPT to meet at the respective sites are shown. The α_6-wheel in gray with PPT and ACP colored in cyan and magenta, respectively. A sphere with a probe radius of 18 Å was used for surface calculation.

critical factor for the appearance of a potential alternative conformation of the *S. cerevisiae* FAS (FAS precomplex). The functional and structural studies suggest that the fungal FAS type I PPT can be active both as a trimer and as a dimer. However, the data do not favor one oligomeric species over the other.

In the FAS complex, the KR and KS domains of the α chain are found in dimeric arrangements, whereas the homologous bacterial counterparts exist in tetrameric and a dimeric oligomerization, respectively (sequence identity of about 24% and 21% to the FAS domains) (Olsen et al., 1999; Price et al., 2001; Qiu et al., 2001; Wang et al., 2006). In light of the oligomeric requirement of the large KR and KS domains, a reactive dimeric PPT species might be favored over the intrinsic trimeric PPT fold. However, a dimeric oligomerization is challenged by the pronounced hydrophobicity of the conserved central channel of the separate PPT, indicating that trimer formation indeed has a physiological relevance and is not just an evolutionary artifact from the related AcpS family. This idea is also supported by the poor conservation of the PPT/KS interface, as observed in the updated FAS model, indicating very low evolutionary pressure on its location in the mature $\alpha_6\beta_6$ complex (see Figure 5B).

Architectural Restraints on a Putative FAS Precomplex

As the position and the dimensions of the pores in the $\alpha_6\beta_6$ arrangement do not favor a catalytically competent interaction between an ACP tethered inside the reaction chamber and a multimeric PPT linked to the C terminus at the outside of the barrel, the activation reaction is unlikely to proceed in the fully assembled FAS complex.

The existence of a separate conformational state in the FAS assembly pathway would well explain the results of earlier experiments. Fichtlscherer et al. (2000) prepared two preparations of nonactivated FAS, one lacking PPT activity by a G1770D mutation and the other carrying an ACP S180A mutation that regained activity when first dissociated and then reassociated in the presence of CoA. Unfortunately, Fichtlscherer and coworkers did not monitor the oligomeric state of the FAS mixture during the reassociation process. However, a similar dissociation/reassociation protocol without addition of CoA was in a previous study observed to produce lower size "additional association products" with KR activity (Werkmeister et al., 1980), indicating a stable α chain containing intermediate.

In light of these results, the naked α_6-wheel would seem to be an appealing candidate as a scaffold responsible for the FAS auto-activation. Since both the ACP and PPT domains are coded on the α chain, the involvement of the β chain might not be necessary. Although the situation for the single chain FAS complexes of, for example, basidiomycetes is hard to predict, the large α-α contacts within the α_6-wheel suggests that the highly homologous α chain equivalent of the single chain FAS might be able to form a similar a hexameric arrangement (Figure S4).

However, even without the β wall and the ACP compartmentalized, the ACP and PPT domains remain separated by a large distance. Given the α_6-architecture, three putative sites for forming a reactive PPT/ACP unit could be envisioned (Figure 7B). Two types of PPT dimers could potentially be formed at two sites on the perimeter of the α_6-wheel, from either dimer- or trimer-related α chains. Interaction of PPT at site 1 is likely to account for the observed ability of $\alpha_6\beta_6$ FAS to phosphopantetheinylate separate ACP. The C-terminal linker of the ACP is 26 residues long, allowing it to stretch ~80 Å from this anchor point at the six-helix bundle at the center of the α_6-wheel. This is not enough to reach a PPT dimer at the perimeter, making both sites 1 and 2 unlikely locations for ACP modification (Figure S5A).

In contrast to dimer formations, a functional PPT trimer, similar to the one seen for the separate PPT domains, could potentially be formed at the three-fold axis of a putative α_6-wheel-based precomplex (site 3, Figure 7B). This would require PPT, but not ACP movements. However, moving the PPT more than 100 Å to the center of the α_6-wheel demands the unwinding of at least 30 residues C-terminal to the KS domain (Figure S5B), also

making interaction site 3 a less likely solution of the FAS activation problem. The activation of the fungal FAS could also potentially occur in an intermolecular reaction of α_6-wheels—for example, in an edge/face arrangement, as shown in Figure 7B. However, considering the orientational constraints in the interactions of, for example, two 1.2 MDa α_6-wheels (Berg and Von Hippel, 1985) and the difficulty in such a reaction mode to modify all ACPs of a wheel before conducting it into the assembly to $\alpha_6\beta_6$ complex, an intermolecular reaction mode seems to be less likely.

With respect to the limitations of an intermolecular activation reaction, and the need for substantial unwinding of secondary structure elements in an intramolecular reaction mode (see Figure 7B), we suggest that the α_6-wheel does not represent the scaffold for the posttranslational modification of ACP. Rather, it seems plausible that the assembly of the *S. cerevisiae* FAS proceeds via a conformation different to the hexameric substructure of the $\alpha_6\beta_6$ FAS. As mentioned above, the β chain is likely not to be critical to the activation process. A precomplex of the α chain without the β chain involved is supported by EM studies on the separate chains showing a distinct substructure of the α chain but not the β chain (Kolodziej et al., 1996).

Implications for the FAS Superfamily

Several examples were reported where fungal FAS type I complexes (sFAS) have evolved to interact with PKSs in secondary metabolic pathways (Brown et al., 1996). These types of FAS complexes are suggested to be differently organized than the $\alpha_6\beta_6$ FAS of primary metabolism (Watanabe and Townsend, 2002). The best-characterized FAS involved in secondary metabolism is the megasynthase of *Aspergillus parasiticus*, which synthesizes the aflatoxin precursor norsolorinic acid. This sFAS/polyketide synthases (PKS) hybrid comprises the subunits HexA and HexB synthesizing a C_6-fatty acid and the PKS PksA further processing this starting compound (Crawford et al., 2008a; Crawford et al., 2008b). The HexA and HexB subunits are highly homologous to the α chain and β chain of the $\alpha_6\beta_6$ FAS (sequence identity α chain/HexA 38%, β-chain/HexB 36%), except that a few structural elements partly involved in the $\alpha_6\beta_6$ assembly are missing. It is tempting to speculate that a precomplex in the assembly pathway of the *S. cerevisiae* FAS and a low-oligomeric structure, as suggested for the secondary metabolite sFAS, might be similar in reflecting alternative and possibly related conformations of fungal FAS systems.

EXPERIMENTAL PROCEDURES

Cloning of the Fungal FAS Type I PPT and ACP Constructs

To express the PPT as separate SUMO-tagged fusion protein, the coding sequence was amplified by PCR using genomic DNA as a template (primers are shown in Table S1). In an In-*fusion* cloning reaction (Clonetech), the gel-purified PCR fragment was assembled with pET28M-SUMO1 (vector kindly provided by the European Molecular Biology Laboratory, Heidelberg), previously digested with BamH I and Hind III, to finally yield the expression plasmids pSuH(6)_PPT.

The His(6)-tagged constructs PPT and ACP were cloned by PCR-amplifying sequences primers shown in Table S1. The gel-purified PCR products and the pET-22b(+) vector (Novagen) were digested with the restriction enzymes Xho I and Nde I and ligated to yield expression plasmids pPPT_H(6) and pACP_H(6). All constructs were confirmed by the dye terminator sequencing method.

Expression and Purification of His(6)-Tagged Constructs

To heterologously express PPT and ACP with noncleavable His(6)-tags (PPT_H(6) and ACP_H(6)) in *E. coli*, plasmids pPPT_H(6) and pACP_H(6) were transformed into BL21 Gold (DE3) cells (Novagen). Single colonies were used to inoculate 35 ml of LB medium containing 100 μg/ml ampicillin and incubated at 37°C for 16 hr; 30 ml were transferred to 3 l of TB medium supplemented with 100 μg/ml ampicillin and grown at 37°C to a density A_{600nm} 0.9. The culture was incubated at 20°C and induced with IPTG (0.5 mM final concentration). After incubation at 20°C for additional 16 hr, cells were harvested, were resuspended in buffer N100 containing 20 mM imidazole, protease inhibitors (Complete Protease Inhibitor Cocktail Tablets, EDTA free, Roche), and DNase (Roche), and were lysed by french press. The lysate was centrifuged for 1 hr at 4°C at 47000 g, and the supernatant was incubated with Ni-NTA Superflow (QIAGEN) for 1 hr at 4°C. During purification with gravity flow columns, the protein was washed at 20 and eluted at 500 mM imidazole. Size exclusion chromatography with a Superdex 200 16/60 column (GE Healthcare) using 20 mM Tris-HCl (pH 7.5), 100 mM NaCl, and 1 mM $MgCl_2$ buffer (buffer N100) was used as final purification step. The proteins were found to be 99% pure, as estimated by SDS-PAGE (Coomassie stained NuPAGE 4%–12% Bis/Tris, Invitrogen).

For purifying PPT under denaturing conditions, urea was added to the cytosolic fraction to reach a final concentration of 8 M. Ni-chelating chromatography was performed as described above with buffers supplemented with urea to 8 M. In order to refold the PPT, pooled elution fractions were concentrated to A_{280nm} 0.5 and dialyzed for 16 hr at 4°C against buffer N100.

PPT Mutants

The PPT mutants—G1770D, V1769D/V1771S/V1773L, V1769D/V1771S/V1773L/V1879S/V1881E, D1772S/E1774S, and R1841A—were derived from the parental plasmid pPPT_H(6) following the QuikChange Site-Directed Mutagenesis Kit (Stratagene). Primers are shown in Table S1. All constructs were confirmed by the dye terminator sequencing method, and all mutants were heterologously expressed in *E. coli* and purified as described above. For the complementation study, PPT mutants D1772S/E1774S and R1841A were separately purified via Ni-chelating chromatography under denaturing conditions, mixed in an equimolar ratio, and finally refolded by dialysis (for purification and refolding, see Expression and Purification of His(6)-Tagged Constructs). All mutants were analyzed by LC-MS on a BRUKER microTOF mass spectrometer (service provided in house by the Core Facility) (see Table 1).

Expression and Purification of the SUMO-PPT Fusion Protein

To heterologously express PPT in *E. coli* as a SUMO fusion protein, plasmid pSuH(6)_PPT was transformed into *E. coli* BL21 Gold (DE3). Ni-chelating chromatography was essentially performed as for His(6)-tagged ACP described above. For cleaving the His(6)-tagged SUMO domain, the protease SenP2 (in house, Core Facility) was added to the pooled elution fraction at A_{280nm} 0.5 (final Sen2P concentration 5 μg/ml). The cleavage was performed overnight at 4°C. Filtration via an equilibrated Ni-NTA Superflow cushion yielded the pure, non-tagged protein. The proteins were further purified via size exclusion chromatography on a Superdex 200 16/60 column (GE Healthcare) using buffer N100.

Expression and Purification of Fungal FAS

The expression and purification of the fungal $\alpha_6\beta_6$ FAS has been described elsewhere (Johansson et al., 2008). For the PPT activity assay, the protein was further purified via a Superose 6 3.2/30 column (GE Healthcare) using buffer N100.

PPT Activity Assay

PPT activity assays were performed in buffer N100 containing 0.3 mM CoA. Concentrations of active centers at 1–2 μM (14 kD per active center for separate PPT; 400 kDa for FAS). After preincubating PPT and CoA for 20 min at 30°C, apo-ACP was added to a final concentration of 35 μM, and the reaction mixture was incubated for another 3 hr. Reactions were finally cooled to 4°C and directly analyzed by LC-MS on a BRUKER microTOF mass spectrometer (service provided in house by the Core Facility). The phosphopantetheine moiety did not affect the ionization properties of the ACP in the mass spectrometric analysis. Thus, the turnover of ACP could be determined by comparing the total ion counts of the deconvoluted MS-spectra of ACP and ACP-SH (see

Table 1). Activity assays of mutant PPTs and mixtures of mutant PPTs (see Table 1) were performed in duplicate. Accordingly, values in Table 1 are means of two values. SDS-PAGE samples of the reaction mixture were prepared immediately after the 3 hr incubation. As a result of disulfide bridging of holo-ACP molecules, the activity of the PPT could also be monitored by SDS-PAGE. For this, ACP was purified from reaction mixture by gel filtration on a Superdex 200 3.2/30 column (see also Figure S1), and kept at 4°C for several days to induce formation of disulfide bridged ACP-SH by oxidation in air. Preparation of SDS-PAGE samples by adding loading buffer without β-mercaptoethanol led to ACP migrating as dimers $(ACP\text{-}S)_2$ (see Figure 4A).

Crystallization

Crystallization conditions were screened in the Crystallization Facility (in house, Department of Structural Cell Biology). Promising conditions were further refined by the hanging drop vapor diffusion method. Diffracting PPT crystals grew at a concentration of 8 mg/ml under 25% PEG 1500 and 0.1 M PCB (sodium propionate/sodium cacodylate/BIS-TRIS propane [2:1:2]; pH 6) at room temperature, and CoA-loaded PPT at concentrations of 8 mg/ml and a molar PPT/CoA ratio of 1:2 under 25% PEG 1500 and 0.1 M MIB (sodium malonate/imidazole/boric acid [2:3:3]; pH 4) at room temperature.

X-Ray Data Collection and Processing

Before flash freezing a crystal in liquid nitrogen, the crystallization drop was flooded with an addition of 2 μl mother liquor acting as a cryo-protectant. X-ray diffraction data of native PPT crystals were collected at the European Synchrotron Radiation Facility (ESRF) beamline ID29 to a resolution of 1.9 Å. The data could be indexed and scaled in $C222_1$ with cell dimensions (92.0 133.7 55.4), giving an R_{merge} of ~18%, but showed strong signs of pseudo-merohedral twinning. Further examination with phenix.xtriage (Afonine et al., 2005) indicated that the crystals instead belonged to $P2_1$ with two twin domains related by a (*l, -k, h*) rotation. The data were rescaled in the monoclinic spacegroup, with cell parameters (81.1 55.8 81.0, 90.0 111.4 90.0) and an R_{merge} of ~7% (see Table 2). Assuming six PPT monomers per asymmetric unit gives a Matthews coefficient of 1.94 $Å^3$/Da, corresponding to a solvent content of 36.7%. Diffraction data of the PPT/CoA complex were collected to a resolution of 2.2 Å, and found to belong to space group C2 with cell dimensions (145.6 73.8 105.7; 130.8), giving a Matthews coefficient of 2.65 $Å^3$/Da with six monomers per asymmetric unit.

Structure Solution

Attempts to solve the native structure using the Cα trace of the integral *S. cerevisiae* FAS PPT domain built at 4 Å (PDB-code 2PFF; Lomakin et al., 2007) failed. Instead, a mosaic model of the *Streptomyces coelicolor* holo-acyl carrier protein synthase (PDB-code 2JCA, unpublished data) was created with SOD (Kleywegt et al., 2001) and was used for molecular replacement in PHASER (McCoy et al., 2007). The top solutions were evaluated by a combination of rigid-body and simulated annealing refinement, using the twin target function of Phenix.refine (Afonine et al., 2005) with a twin fraction of 0.31. The best model was rebuilt and subjected to individual coordinate and *B* factor twin refinement in Phenix. After each cycle of refinement, the σ_A-weighted $2F_o\text{-}F_c$ and $F_o\text{-}F_c$ maps were used for further rebuilding in O (Jones et al., 1991) and Coot (Emsley and Cowtan, 2004). Water molecules were added using the ordered_solvent function of Phenix.refine and Coot, in peaks (>1.5) of the $2F_o\text{-}F_c$ electron density map. Superimposing the final PPT model onto the Cα trace of the low-resolution FAS PPT domain (Lomakin et al., 2007) results in an RMSD of 1.7 Å. This should be compared with a superposition of any of the bacterial AcpS enzymes over the same range, resulting in an RMSD between 1.2 and 1.8 Å. The structure of the PPT/CoA complex was solved by PHASER (McCoy et al., 2007), using the high-resolution FAS PPT structure as a search model and refined with Phenix.refine (Afonine et al., 2005) (see Table 2). The high resolution PPT domain and a polyalanine model of helix α52 was placed into the 4 Å structure of the *S. cerevisiae* FAS complex (PDB-code 2VKZ; Johansson et al., 2008) and was subjected to rigid-body and TLS refinement in Phenix.refine (Afonine et al., 2005). The full FAS/PPT model has been deposited at the Protein Data Bank with accession code 3HMJ.

Structural alignments were made using Coot and the Lsq tools of O (Jones et al., 1991), and structure-based sequence alignments were made using the INDONESIA package (D. Madsen, P. Johansson, and G. J. Kleywegt, unpublished data). Molecular figures were made in PYMOL (www.pymol.org). Coordinates and structure factors of the FAS type I PPT domain and the FAS type I PPT/CoA complex have been deposited at the Protein Data Bank with codes 2WAS and 2WAT, respectively.

Table 2. Data Collection and Refinement Statistics

	FAS type I PPT	FAS type I PPT/CoA
Data collection		
Space group	$P2_1$	C2
Cell dimensions	*a* = 81.1 Å, *b* = 55.8 Å, *c* = 81.0 Å, β = 111.4°	*a* = 145.6 Å, *b* = 73.8 Å, *c* = 105.7 Å, β = 130.8°
Resolution (Å)	75.6–1.9 (2.0)[a]	80.1–2.2 (2.31)[a]
R_{merge}	0.069 (0.62)	0.096 (0.40)
$< I / \sigma I >$	12.0 (2.1)	12.2 (2.6)
Completeness (%)	99.6 (90.0)	97.9 (89.0)
Redundancy	3.6 (3.4)	3.7 (3.5)
Refinement		
Resolution (Å)	31.3–1.9	25.0–2.2
Measured / unique refl.	498054 / 53109	156218 / 42185
R_{work} / R_{free}	0.218 / 0.254[b]	0.217 / 0.252
No. atoms		
Protein	4960	5622
Water	194	505
Ligand		239
Average *B*-factors		
Protein ($Å^2$)	42.9	29.4
Water ($Å^2$)	39.0	34.5
Ligand ($Å^2$)		28.8
Ramachandran outliers (%)	1.2	1.3
R.m.s deviations		
Bond lengths (Å)	0.010	0.006
Bond angles (°)	1.1	1.04

[a] Values in parentheses refer to highest-resolution shell.
[b] As given by the twin target function of Phenix.refine (Afonine et al., 2005) with a twin fraction of 0.31.

ACCESSION NUMBERS

Coordinates and structure factors of the FAS type I PPT and the FAS type I PPT in complex with CoA have been deposited at the Protein Data Bank with codes 2was and 2wat, respectively. A refined and updated *Saccharomyces cerevisiae* FAS model has been deposited with the code 3hmj.

SUPPLEMENTAL DATA

Supplemental Data include five figures and one table and can be found with this article online at http://www.cell.com/structure/supplemental/S0969-2126(09)00256-1.

ACKNOWLEDGMENTS

The expression plasmid pET28M-SUMOI was kindly provided by the European Molecular Biology Laboratory Heidelberg. Our sincere thanks go to the Core Facility (in house), particularly to Lissy Weyher-Stingl, for providing mass spectrometric analysis of apo- and holo-ACPs, and to the Crystallization Facility (in house, Department of Structural Cell Biology), particularly to Karina

Valer-Saldana and Jerome Basquin. We are also grateful to Anuschka Pauluhn (SLS, Villigen), Joanne McCarthy and Didier Nurizzo (ESRF, Grenoble) for beamline support, Ursel Grampp-Heider for organization of the laboratory, and Mike Dyall-Smith and Kosta Konstantinidis for reading and discussing the manuscript. We finally thank the referees for thorough and constructive comments on the manuscript during the revision process.

Received: March 2, 2009
Revised: June 30, 2009
Accepted: June 30, 2009
Published: August 11, 2009

REFERENCES

Afonine, P.V., Grosse-Kunstlev, R.W., and Adams, P.D. (2005). The Phenix refinement framework. CCP4 Newsletter, *8*.

Berg, O.G., and Von Hippel, P.H. (1985). Diffusion-controlled macromolecular interactions. Annu. Rev. Biophys. Biophys. Chem. *14*, 131–160.

Boulanger, R.R., and Kantrowitz, E.R. (2003). Characterization of a monomeric *E. coli* alkaline phosphatase formed upon a single amino acid substitution. J. Biol. Chem. *278*, 23497–23501.

Brown, D.W., Adams, T.H., and Keller, N.P. (1996). Aspergillus has distinct fatty acid synthases for primary and secondary metabolism. Proc. Natl. Acad. Sci. USA *93*, 14873–14877.

Bunkoczi, G., Pasta, S., Joshi, A., Wu, X., Kavanagh, K.L., Smith, S., and Oppermann, U. (2007). Mechanism and substrate recognition of human holo ACP synthase. Chem. Biol. *14*, 1243–1253.

Chakravarty, B., Gu, Z., Chirala, S.S., Wakil, S.J., and Quiocho, F.A. (2004). Human fatty acid synthase: structure and substrate selectivity of the thioesterase domain. Proc. Natl. Acad. Sci. USA *101*, 15567–15572.

Chirgadze, N.Y., Briggs, S.L., McAllister, K.A., Fischl, A.S., and Zhao, G. (2000). Crystal structure of *Streptococcus pneumoniae* acyl carrier protein synthase: an essential enzyme in bacterial fatty acid biosynthesis. EMBO J. *19*, 5281–5287.

Chopra, S., Kumar Singh, S., Prasad Sati, S., Ranganathan, A., and Sharma, A. (2002). Expression, purification, crystallization and preliminary X-ray analysis of the acyl carrier protein synthase (AcpS) from *Mycobacterium tuberculosis*. Acta Crystallogr. D Biol. Crystallogr. *58*, 179–181.

Copp, J.N., and Neilan, B.A. (2006). The phosphopantetheinyl transferase superfamily: phylogenetic analysis and functional implications in cyanobacteria. Appl. Environ. Microbiol. *72*, 2298–2305.

Crawford, J.M., Vagstad, A.L., Ehrlich, K.C., Udwary, D.W., and Townsend, C.A. (2008a). Acyl-carrier protein-phosphopantetheinyltransferase partnerships in fungal fatty acid synthases. ChemBioChem *9*, 1559–1563.

Crawford, J.M., Thomas, P.M., Scheerer, J.R., Vagstad, A.L., Kelleher, N.L., and Townsend, C.A. (2008b). Deconstruction of iterative multidomain polyketide synthase function. Science *320*, 243–246.

Ehmann, D.E., Gehring, A.M., and Walsh, C.T. (1999). Lysine biosynthesis in *Saccharomyces cerevisiae*: mechanism of alpha-Aminoadipate Reductase (Lys2) involves posttranslational phosphopantetheinylation by Lys5. Biochemistry *38*, 6171–6177.

Elovson, J., and Vagelos, P.R. (1968). Acyl carrier protein. X. Acyl carrier protein synthetase. J. Biol. Chem. *243*, 3603–3611.

Emsley, P., and Cowtan, K. (2004). Coot: model-building tools for molecular graphics. Acta Crystallogr. D. Biol. Crystallogr *60*, 2126–2132.

Fichtlscherer, F., Wellein, C., Mittag, M., and Schweizer, E. (2000). A novel function of yeast fatty acid synthase. Subunit alpha is capable of self-pantetheinylation. Eur. J. Biochem. *267*, 2666–2671.

Jenni, S., Leibundgut, M., Boehringer, D., Frick, C., Mikolasek, B., and Ban, N. (2007). Structure of fungal fatty acid synthase and implications for iterative substrate shuttling. Science *316*, 254–261.

Johansson, P., Wiltschi, B., Kumari, P., Kessler, B., Vonrhein, C., Vonck, J., Oesterhelt, D., and Grininger, M. (2008). Inhibition of the fungal fatty acid synthase type I multienzyme complex. Proc. Natl. Acad. Sci. USA *105*, 12803–12808.

Jones, T.A., Zou, J.Y., Cowan, S.W., and Kjeldgaard, M. (1991). Improved methods for building protein models in electron density maps and the location of errors in these model. Acta Crystallogr. A. *47*, 110–119.

Joshi, A.K., Zhang, L., Rangan, V.S., and Smith, S. (2003). Cloning, expression, and characterization of a human 4′-phosphopantetheinyl transferase with broad substrate specificity. J. Biol. Chem. *278*, 33142–33149.

Keating, M.-M., Gong, H., and Byers, D.M. (2002). Identification of a key residue in the conformational stability of acyl carrier protein. Biochim. Biophys. Acta. *1601*, 208–214.

Kleywegt, G.J., Zou, J.Y., Kjeldgaard, M., and Jones, T.A. (2001). Around O. In International Tables for Crystallography, Vol. F. Crystallography of Biological Macromolecules, M.G. Rossmann and E.V. Arnold, ed. (Dordrecht, The Netherlands: Kluwer Academic Publishers), pp. 353–356.

Kolodziej, S.J., Penczek, P.A., Schroeter, J.P., and Stoops, J.K. (1996). Structure-function relationships of the *Saccharomyces cerevisiae* fatty acid synthase. Three-dimensional structure. J. Biol. Chem. *271*, 28422–28429.

Lambalot, R.H., and Walsh, C.T. (1995). Cloning, overproduction, and characterization of the *Escherichia coli* holo-acyl carrier protein synthase. J. Biol. Chem. *270*, 24658–24661.

Lambalot, R.H., Gehring, A.M., Flugel, R.S., Zuber, P., LaCelle, M., Marahiel, M.A., Reid, R., Khosla, C., and Walsh, C.T. (1996). A new enzyme superfamily—the phosphopantetheinyl transferases. Chem. Biol. *3*, 923–936.

Leibundgut, M., Jenni, S., Frick, C., and Ban, N. (2007). Structural basis for substrate delivery by acyl carrier protein in the yeast fatty acid synthase. Science *316*, 288–290.

Lomakin, I.B., Xiong, Y., and Steitz, T.A. (2007). The crystal structure of yeast fatty acid synthase, a cellular machine with eight active sites working together. Cell *129*, 319–332.

Lynen, F. (1980). On the structure of fatty acid synthetase of yeast. Eur. J. Biochem. *112*, 431–442.

Maier, T., Leibundgut, M., and Ban, N. (2008). The crystal structure of a mammalian fatty acid synthase. Science *321*, 1315–1322.

McCoy, A.J., Grosse-Kunstleve, R.W., Adams, P.D., Winn, M.D., Storoni, L.C., and Read, R.J. (2007). Phaser crystallographic software. J. Appl. Crystallogr. *40*, 658–674.

Olsen, J.G., Kadziola, A., Von Wettstein-Knowles, P., Siggaard-Andersen, M., Lindquist, Y., and Larsen, S. (1999). The x-ray crystal structure of beta-ketoacyl [acyl carrier protein] synthase I. FEBS Lett. *460*, 46–52.

Parris, K.D., Lin, L., Tam, A., Mathew, R., Hixon, J., Stahl, M., Fritz, C.C., Seehra, J., and Somers, W.S. (2000). Crystal structures of substrate binding to *Bacillus subtilis* holo-(acyl carrier protein) synthase reveal a novel trimeric arrangement of molecules resulting in three active sites. Structure *8*, 883–895.

Ploskon, E., Arthur, C.J., Evans, S.E., Williams, C., Crosby, J., Simpson, T.J., and Crump, M.P. (2008). A mammalian type I fatty acid synthase acyl carrier protein domain does not sequester acyl chains. J. Biol. Chem. *283*, 518–528.

Price, A.C., Zhang, Y.M., Rock, C.O., and White, S.W. (2001). Structure of beta-ketoacyl-[acyl carrier protein] reductase from *Escherichia coli*: negative cooperativity and its structural basis. Biochemistry *40*, 12772–12781.

Qiu, X., Janson, C.A., Smith, W.W., Head, M., Lonsdale, J., and Konstantinidis, A.K. (2001). Refined structures of beta -ketoacyl-acyl carrier protein synthase III. J. Mol. Biol. *307*, 341–356.

Reuter, K., Mofid, M.R., Marahiel, M.A., and Ficner, R. (1999). Crystal structure of the surfactin synthetase-activating enzyme Sfp: a prototype of the 4′-phosphopantetheinyl transferase superfamily. EMBO J. *18*, 6823–6831.

Roujeinikova, A., Baldock, C., Simon, W.J., Gilroy, J., Baker, P.J., Stuitje, A.R., Rice, D.W., Slabas, A.R., and Rafferty, J.B. (2002). X-ray crystallographic studies on butyryl-ACP reveal flexibility of the structure around a putative acyl chain binding site. Structure *10*, 825–835.

Schweizer, E., and Hofmann, J. (2004). Microbial type I fatty acid synthases (FAS): major players in a network of cellular FAS systems. Microbiol. Mol. Biol. Rev. *68*, 501–517.

Spivey, H.O., and Ovadi, J. (1999). Substrate channeling. Methods *19*, 306–321.

Vedadi, M., Lew, J., Artz, J., Amani, M., Zhao, Y., Dong, A., Wasney, G.A., Gao, M., Hills, T., Brokx, S., et al. (2007). Genome-scale protein expression and structural biology of *Plasmodium falciparum* and related Apicomplexan organisms. Mol. Biochem. Parasitol. *151*, 100–110.

Wang, J., Soisson, S.M., Young, K., Shoop, W., Kodali, S., Galgoci, A., Painter, R., Parthasarathy, G., Tang, Y.S., Cummings, R., et al. (2006). Platensimycin is a selective FabF inhibitor with potent antibiotic properties. Nature *441*, 358–361.

Watanabe, C.M.H., and Townsend, C.A. (2002). Initial characterization of a type I fatty acid synthase and polyketide synthase multienzyme complex NorS in the biosynthesis of alfatoxin B1. Chem. Biol. *9*, 981–988.

Werkmeister, K., Wieland, F., and Schweizer, E. (1980). Coenzyme A: fatty acid synthetase apoenzyme 4′-phosphopantetheine transferase in yeast. Biochem. Biophys. Res. Commun. *96*, 483–490.

Zhang, Y.-M., Marrakchi, H., White, S.W., and Rock, C.O. (2003). The application of computational methods to explore the diversity and structure of bacterial fatty acid synthase. J. Lipid Res. *44*, 1–10.

